A Study of Molecular Dynamics and Energy Transfer within Derivitized Benzo-Crown Ethers

by
Tyler A. Elias

A senior thesis submitted
to the
Department of Chemistry
in partial fulfillment of
the requirements for the
Degree of Bachelor of Science
with Honors

University of Michigan
Ann Arbor, Michigan 48109 USA
April 23, 2013

Forward

As I begin to write my Senior Thesis, I cannot help but reflect upon my last four years here at the University of Michigan. While I fully expected to learn a great deal about chemistry and neighboring fields, which I certainly have, what I really found is that this education has given me a profoundly new view on life and the world we live in. Having the chance to gain some understanding of and to manipulate the very essence of existence, whether it molecular matter, light, or other energy, has been thrilling and troubling, but nonetheless satisfying. These experiences have played a tremendous role in how I define myself and the goals I have set; I am undoubtedly better off for them.

However, none of this could have been possible if it weren't for the support I received from many important people. First and foremost are my parents, Leonard and Rhonda Elias. They instilled within me ambition and the drive to always do my best and to make it count, while providing the love and support necessary to achieve. My Aunt Jan, who is like a second mother, has also taken on many of these roles and has given me one more person I can always count on. Megan, my younger sister, has been an indispensable part of my life for the past fourteen years. She has given me a reason to be accountable, has taught me how to teach, be calm and understanding, and has given me reassurance through her love and admiration.

As for my formal education, there are countless contributors but a few stand out from the rest. I would like to thank my kindergarten and elementary science teacher Mary Thompson for my early love of science and encouraging my inquisitive nature. In high school, Rosanne Macksoud, Sue Young, and Keith Yenior gave me my first chemistry and physics lessons which attracted me to the field and bolstered my curiosity and ability to question. Professors Koreeda, Hakansson, Pecoraro, and Kubarych were all highly influential here at the University and I

consider myself lucky to have been a student of these truly gifted and insightful teachers. I would also like to thank Dr. Kubarych further for his attentive and inspirational mentorship, along with those in his research group, including Aaron White and Josef Dunbar in particular. These three formed an essential support base for this research project, providing me with the necessary knowledge and skills while being a reliable resource for ideas and brainstorming. Finally, I am infinitely grateful to the University of Michigan and the supporters of the Frederick G.L. Huetwell Scholarship for funding my college education, which has given me an incalculable advantage as I transition into the working world.

Table of Contents

Forward i

Chapter 1: Motivation and Background 1

- Abstract 1
- Introduction 1
- Molecular Background 2

Chapter 2: Experimental Methods 4

- Synthesis and Characterization 4
  - Final Procedure 4
  - Additional Notes 5
  - NMR Evaluation 6
- Computational Chemistry 10
- Fourier-Transform Infrared Spectroscopy 12

Chapter 3: Results & Discussion 12

Chapter 4: Two-Dimensional Infrared Experimentation 20

- 2DIR Background 20
- Experimental Set-up 22
- Proposed Experiments 23

Chapter 5: Conclusion 24

References 25

Chapter 1: Motivation and Background

1.1 Abstract

Due to their unique structural properties, benzo-crown ethers are a particularly interesting family of molecules for applications in the optical sensing of chemical systems. This project aims to create a better understanding of the energetic mechanisms by which these probes function through the implementation of computational studies, Fourier-Transform Infrared Spectroscopy, and Two-Dimensional Infrared Spectroscopy. Specifically, $Cr(CO)_3(\eta^6$-benzo-18-crown-6)-Na(SCN) along with several variations were emphasized in order to paint a complete picture of the complex interactions which take place. The $Cr(CO)_3$ reporting group was found to be highly sensitive to minute changes in its environment, with through-molecule and possible through-solvent modes contributing. Unfortunately, due to complications with the laser, the likely more telling Two-Dimensional experiments could not be completed in time to be reported here, but these works will serve these future endeavors well.

1.2 Introduction

The chemistry of crown ethers has received considerable multi-disciplinary attention due to their ability to characteristically bind various cations, including Na^+, K^+, and hydrated protons.[1,2,3] When joined with a "conducting" arene group and an optically active reporting group, crown ethers become quite effective ion sensors via infrared spectroscopy and Nuclear Magnetic Resonance Spectrometry (NMR). In this case, the model system $Cr(CO)_3(\eta^6$-benzo-18-crown-6)-Na(SCN) was chosen as the focus of the study due to the sharp absorptions in the IR, the small frequency difference between the CO and SCN absorption bands which is necessary for spectroscopy experiments, and the versatility of the crown in binding cations.[1,3] Instances of proven preliminary applications using similar molecules include straight-forward pH and ion

concentration sensing in solution.[1,4] However, it is easy to imagine more developed applications studying important biological pathways since a great deal of cellular activity is driven by trans-membrane proton gradients and Na^+/K^+ transportation.[3] In order to reach this level of detail, it is important to gain a mechanistic understanding of how chemical information is relayed to the optical reporting groups. This work aims for that goal through the use of computational calculations, Fourier Transform Infrared Spectroscopy (FTIR) studies, and eventual Two-Dimensional Infrared Spectroscopy (2DIR) experiments.

1.3 Molecular Background

Crown ethers exhibit chelation via non-bonding electrons on the oxygen atoms within the crown, which have been shown to bind cations and the overall size of the cavity dictates the favorability for each (see figure 1). For instance, 18-crown-6 readily binds hydronium but cannot accommodate higher order hydrates such as $H_5O_2^+$ due to steric inhibitions, but 24-crown-8 may.[3] Similar trends have been studied with monovalent cations, Li^+, Na^+, K^+, etc.[5] Having been isolated and examined by X-ray crystallography,[1] many of these crown-ion complexes are also quite stable.

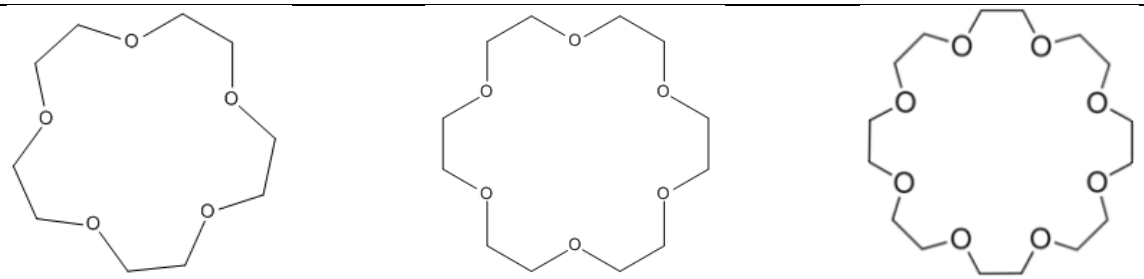

15-crown-5 18-crown-6 24-crown-8

Figure 1. Structures of common crown ethers. Note the Members-Crown-Oxygen nomenclature.

Adding a benzene ring to these basic crown structures allows for the export of chemical information through the conjugated arene system. The electron-rich p-orbitals of the carbon atoms also serve as an excellent ligand by which a metal-carbonyl reporting group may be

synthetically attached. Here, $Cr(CO)_3(\eta^6$-benzo-18-crown-6) (see figure 2) was chosen for its ease of synthesis, stability upon completion, and its ability for application to a number of cations. Chromium tricarbonyl is a particularly useful reporting group because of the carbonyl's three stretching modes which absorb strongly in the 1800-2100 cm^{-1} region. These modes, comprised of one symmetric stretch of A_1 symmetry and two degenerate asymmetric E-symmetry stretches, are known to shift or break degeneracy in certain chemical environments. These reactions are quite sensitive given the back-bond-dependent nature of the chromium-carbonyl bonds. For instance, the presence of a cation in the cavity of the crown would be expected to withdraw electron density away from the chromium and thus out of the C-O π^*-antibonding orbitals.[1] This evacuation increases the overall bonding character of the groups and subsequently increases their vibrational frequencies. Any addition may also disrupt the symmetry of the asymmetric modes, causing peak splitting and the overall band to broaden. This transition is indeed the most tell-tail indicator of the molecule's overall environment.

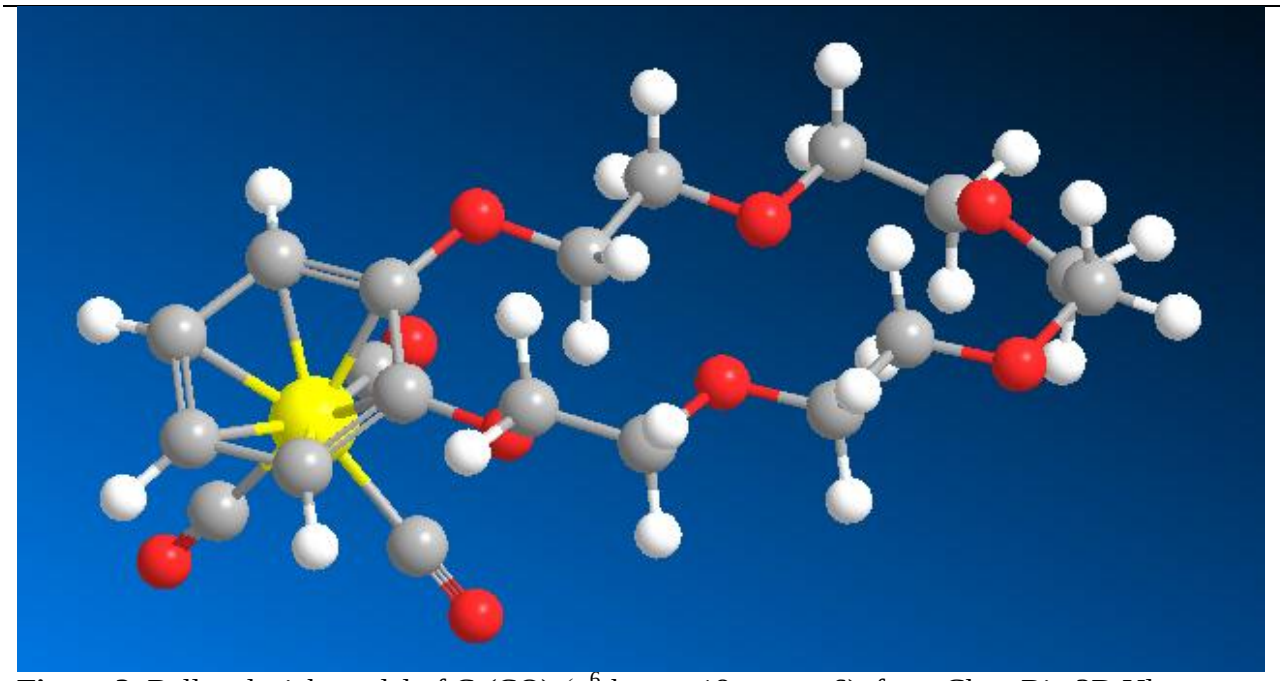

Figure 2. Ball and stick model of $Cr(CO)_3(\eta^6$-benzo-18-crown-6), from ChemBio 3D Ultra

Chapter 2: Experimental Methods

2.1 Synthesis and Characterization

Final Procedure

This synthesis procedure was based on the findings of Shriver,[6] Toma,[7,8,9] and Jaouen,[10] in addition to further experimentation. Benzo-18-crown-6 (3 mmol, 0.9372 g) and $Cr(CO)_6$ (3 mmol, 0.6622 g) were dissolved together in a 90:10 dibutyl ether : tetrahydrofuran (THF) solvent system (80 mL) within a 100 mL single-necked roundbottom flask. This apparatus was equipped with a small magnetic stirbar, long straight-tubed jacketed condenser topped with a 2-opening pressure adapter. The screw-controlled opening was connected to a small water bubbler and the other, permanently open acceptor was connected to one port of a Schlenk line. The reaction vessel was then alternately evacuated and flushed with nitrogen three times per standard Schlenk procedure. With nitrogen flowing to the vessel and through the small bubbler, the Schlenk line was closed to maintain a nitrogen atmosphere while the bubbler port remained open to allow for the escape of reaction gasses. The reaction system was then refluxed in an oil bath at an oil temperature of 140 °C for 20 hours with mild stirring. After this period, the solution turns from clear to yellow, signifying the coordination of chromium. When cooled to room temperature, the stirbar was removed and the resulting solution was rotary evaporated at a bath temperature of 60 °C under medium-high aspirator vacuum pressure. With the removal of the solvent a yellow-green solid persists (see figure 3). This solid was then redissolved in methanol and run through a short (approx. 4 cm) silica column with additional methanol under controlled nitrogen pressure, recovering as much yellow chromium complex as possible. This process removes any oxidized chromium species (green and brown), leaving them at the top of the column. The yellow, chromium-complex containing fractions were then recombined and rotary evaporated under low

aspirator pressure and at a bath temperature of 40 °C. This change in conditions takes into account the lower boiling point of methanol compared to dibutyl ether. Bright yellow flakes result (see figure 3). These flakes were subsequently washed thoroughly with 1:1 diethyl ether : acetone to remove the uncomplexed benzo-18-crown-6 (henceforth referred to as MB6 for mono-benzo, 6-oxygen), resulting in sparkling yellow crystals. These reaction and purification steps were monitored by NMR to ensure identity and purity.

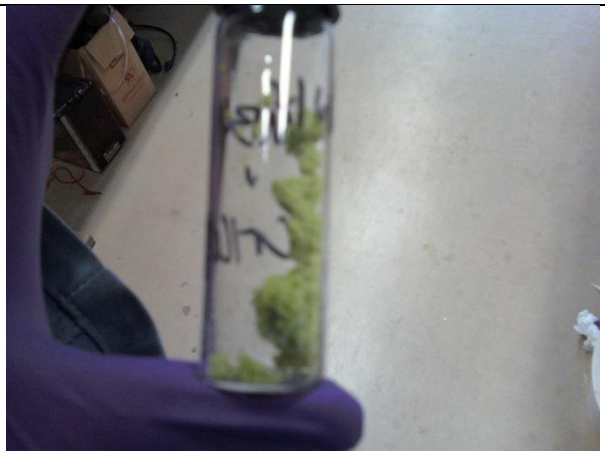

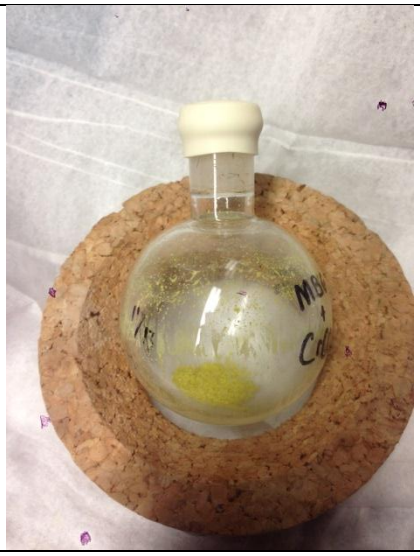

Figure 3. Above: Pre-column Product
Right: Post-Column product

Additional Synthesis Notes

Several reaction apparatus configurations were tested before arrival at the solution described above. A 2-necked roundbottom flask and a continuous flow of nitrogen from the bottom though the bubbler was tried in hopes of encouraging the evolution of CO as $Cr(CO)_6$ coordinated to the benzene ring. However, this only encouraged the escape of refluxing solvents and subliming $Cr(CO)_6$ and resulted in reaction incompletion. It was also important to use a straight tubed condenser. A ribbed condenser may increase solvent condensation but makes washing back deposited $Cr(CO)_6$ more difficult. It is also important to cool the reaction under a

flow of nitrogen in order to reduce the chance for oxidation and to fill the resulting vacuum with something other than water from the attached bubbler.

NMR Evaluation

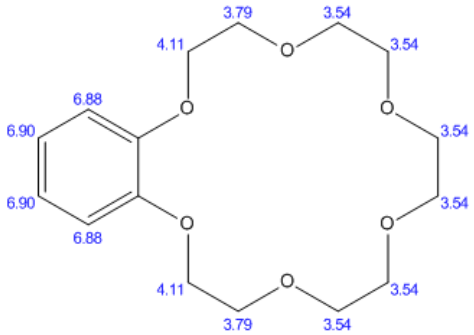

Figure 4. Predicted ^{1}H-NMR chemical shifts (left) and spectrum (below) for benzo-18-crown-6 in $CDCl_3$, as calculated by ChemDraw.

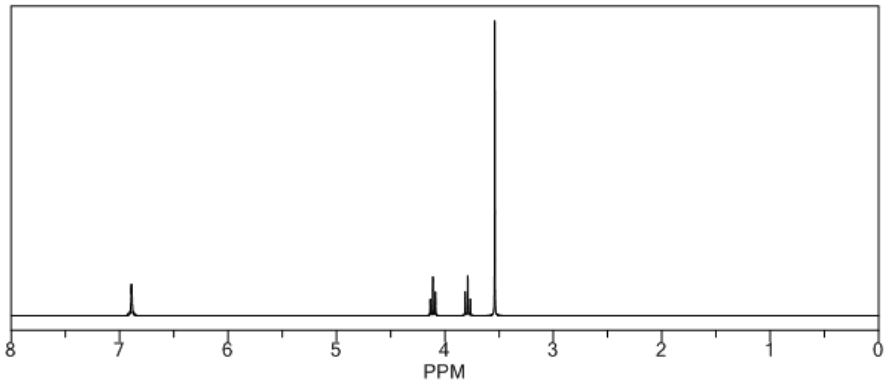

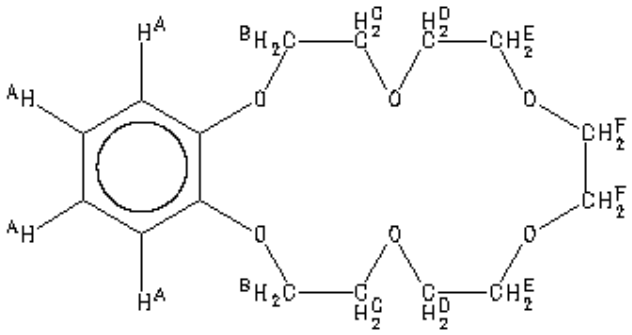

Assign.	Shift (ppm)
A	6.95 to 6.82
B	4.157
C	3.925
D	3.770
E	3.720
F	3.686

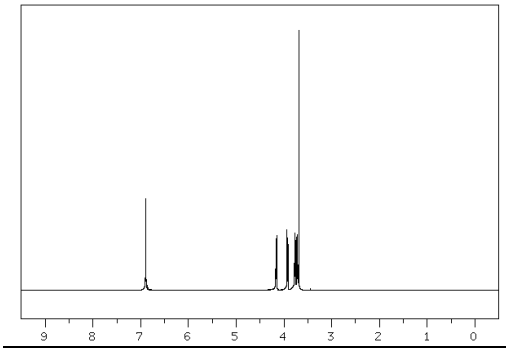

Figure 5. Reported ^{1}H-NMR chemical shifts (above) and spectrum (left) for benzo-18-crown-6 in $CDCl_3$, courtesy of SDBS online.

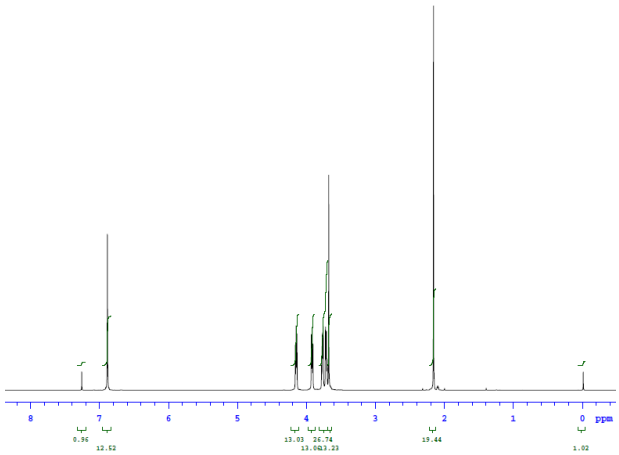

Figure 6. Measured ^{1}H-NMR spectrum of pure benzo-18-crown-6 in $CDCl_3$.

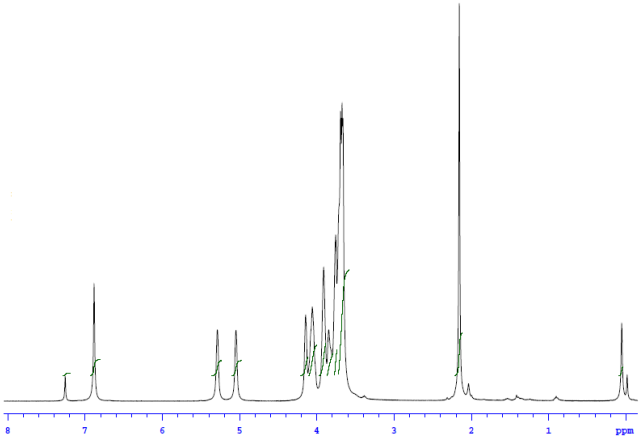

Figure 7. Measured ^{1}H-NMR spectrum of complexed product, post column, pre wash, in $CDCl_3$

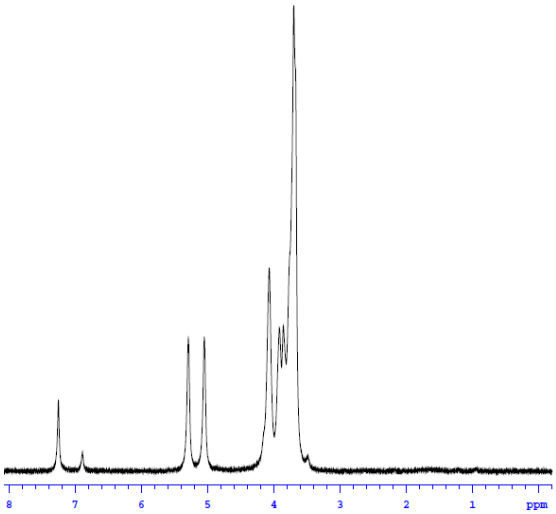

Figure 8. Measured ^{1}H-NMR spectrum of complexed product, post wash, in $CDCl_3$

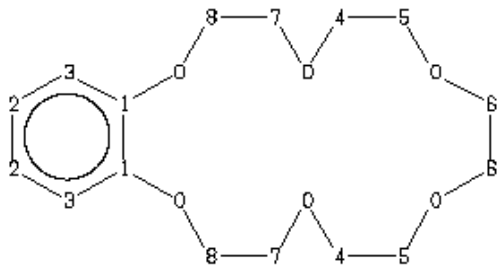

ppm	Int.	Assign.
149.21	313	1
121.53	517	2
114.59	368	3
70.86	1000	4
69.79	492	7
69.25	454	8

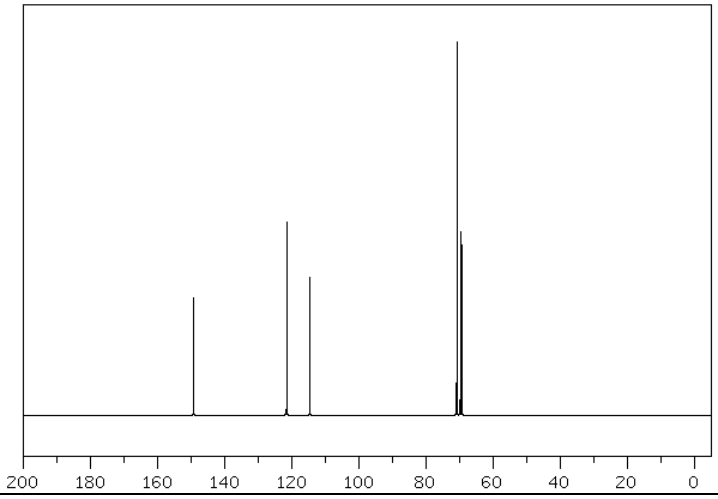

Figure 9. Reported ^{13}C-NMR chemical shifts (above) and spectrum (left) of benzo-18-crown-6 in $CDCl_3$, courtesy of SDBS online.

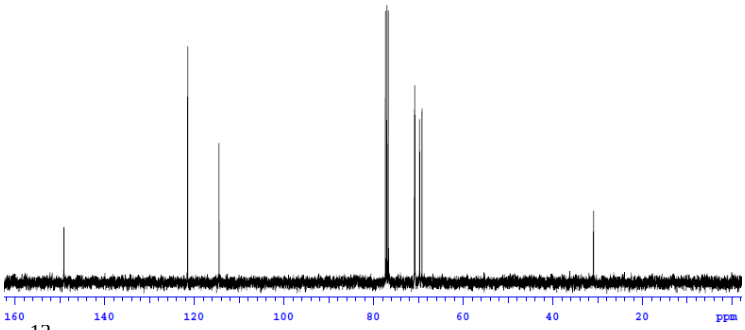

Figure 10. Measured ^{13}C-NMR spectrum of pure benzo-18-crown-6 in $CDCl_3$.

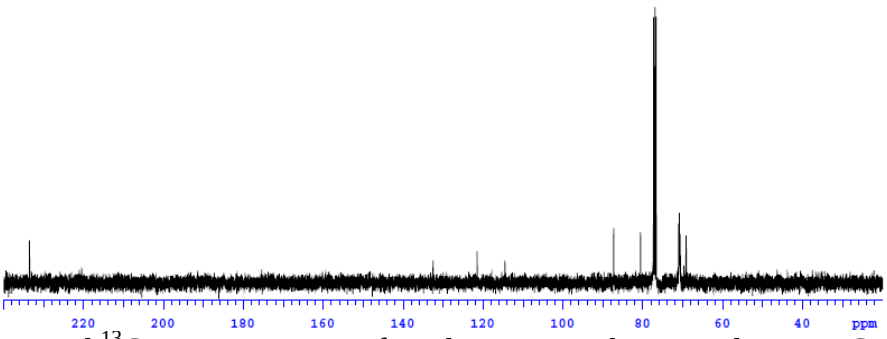

Figure 11. Measured ^{13}C-NMR spectrum of product, pre-wash, post column, in $CDCl_3$

NMR is based on measuring transitions in nuclear spin states induced by the absorption of circularly polarized electromagnetic radiation. Nuclei with spin quantum I = ½, such as ^{1}H and ^{13}C, are particularly useful in that they only have two spin states between which to transition, namely m = +½ and m = -½. When an external magnetic field is applied to a sample, these spin states break degeneracy, with a slightly higher population in the lower energy state. The magnetic dipole of the nucleus processes around the axis of the external magnetic field either with or against the field vector, corresponding to the lower or higher energy state, respectively. This procession occurs at a characteristic Larmor Frequency. When the frequency of the circularly polarized radiation produced by the instruments RF oscillator matches the Larmor frequency of a nucleus, that nucleus absorbs the radiation and flips magnetic spin states, resulting in detection.[11] On the above spectra, a higher frequency corresponds to a lower ppm (δ) value.

In the case of the synthesis at hand, a 400 MHz NMR was used to collect spectra of samples in $CDCl_3$. The important peaks to take note of are in the proton spectra at δ = 6.89, 5.30, and 5.06 ppm. The singlet at 6.89 ppm (figures 5-8) corresponds to the four aromatic hydrogen atoms on the benzene ring. Without coordination of chromium tricarbonyl, all four are nearly chemically identical. Post reaction, however, the single peak splits into the latter two named above, which correspond to two groups of hydrogen atoms, the two closest to the crown and the two furthest away. This split is due to a geometry and orbital hybridization change in the connecting oxygen atoms, which allow for enhanced coupling with the arene π-system,[1] and will be discussed in further detail in subsequent sections. The significant ~2 ppm up-field chemical shift may be explained by a combination of increased electronic shielding and disruption of induced ring currents. With the addition of chromium to the π-system, electron density around these protons is greatly increased. Circulating electrons create local magnetic fields which, in the

case of protons, typically oppose the applied external field, requiring a higher frequency for resonance.[11] Also, coordination with chromium disrupts the free conjugation of the benzene ring. In a free ring, the applied magnetic field through the ring induces a current around the π-system, similar to a magnetic field through a wire ring. This current then creates a local magnetic field which opposes the applied field in the center of the ring but adds on the outside of the ring where the hydrogen atoms exist. Therefore, a lower external field is required to bring them into resonance.[11] If the π-system is altered, however, this effect may be reduced or cancelled, bringing about an up-field chemical shift for the aromatically linked protons. Similar chemical shifts, although much less pronounced, are also exhibited in the crown hydrogen atoms around $\delta = 4.0$, suggesting direct electronic coupling with the chromium tricarbonyl addition.

One may easily track the purification progress based on these principles. In comparing the spectra in figures 7 and 8, the peak at $\delta = 6.89$ almost nearly disappears, as does the extra set of crown hydrogen atoms, signifying a significant purification. Other important peaks to identify are at $\delta = 0.0$ and 7.29 ppm, which are from TMS internal standard and $CDCl_3$ solvent, respectively. A singlet corresponding to acetone at $\delta = 2.18$ also appears in figures 6 and 7, which is residual from test tube cleaning. The ^{13}C-NMR spectra may also be used for purification monitoring but take considerably more time to collect and typically exhibit a lower signal-to noise ratio. However, they are applicable for structure validation; the coordinated carbonyls are clearly evident in figure 11 at $\delta = 234$ ppm.

2.2 Computational Chemistry

Several computational chemistry calculations were run based on Density Functional Theory (DFT) using the Gaussian 09 program suite. Initial geometries were calculated using MM2 force field energy optimization within CambridgeSoft ChemBio3D Ultra. Specifically,

molecular geometries were energetically optimized and IR vibration modes and molecular orbitals were calculated for comparison among many different relevant species in hopes of gaining information about molecular dynamics and vibrational coupling between the carbonyls and thiocyanate. For all atoms the b3lyp/6-31+G(d) functional/basis set was employed except chromium, for which b3lyp/lanl2dz was selected. The former basis set was chosen based on the necessity to include polarization and diffuse functions in this molecular system. The (d) adds a set of six second-order polarization functions, or five standard d-orbitals and one additional s-orbital, to what is strictly necessary to describe stand-alone main-block atoms in their ground state.[12] This addition aids in aptly describing hypervalent or abnormally bonded atoms, such as the sulfur and sodium atoms in these systems. Diffuse functions work to more accurately define electron density at long distances from nuclei and are important when dealing with ionic interactions.[13,14] Lanl2dz implements an effective potential for core electrons which saves processor time.[15] This is useful for chromium because it is such a large atom and the core electrons play little part in the overall reactivity of the molecule. Unless otherwise noted, all calculations were done in vacuum to emphasize target trends. Some calculations were completed in a simulated solvent (THF) environment for comparison using the Polarizable Continuum Model (PCM) and starting from geometries previously optimized in vacuum. Molecular orbitals were calculated using Natural Bond Orbital Theory (NBO) and were visualized using Molden. In order to gain a picture of the dependence of electron density and vibrational coupling on the thiocyanate group, a modredundant optimization was carried out by stepping the moiety around the crown about a central dihedral angle in increments of 36° for 5 steps (six total positions), optimizing the geometry at each, to be followed by subsequent calculations of molecular orbitals

and vibrational frequencies. All calculated vibrational frequencies were multiplied by the suggested basis-set dependent correction factor of 0.9613.[15,16]

2.3 Fourier Transform Infrared Spectroscopy

FT-IR absorbance spectra were collected from a number of relevant samples in order to compare with computational data to find trends in asymmetric peak splitting and vibrational frequency shifts, which will ultimately allow for effective 2DIR experiments. All samples were dissolved in THF and were placed between CaF_2 windows separated by thin Teflon spacers for transmission analysis by a Jasco FT/IR 4100 series instrument. Analyte solutions were approximately 30 mM concentrations; ions were added to form complexes at a 1:1 ratio. Resulting data was imported into Matlab R2009a where it was smoothed and fit using Gaussian functions to determine peak center shifts and splitting of asymmetric carbonyl modes. Care was taken to ensure proper fitting and frequency reporting by setting reasonably limited ranges of function amplitudes, center lines, and widths (Gaussian function terms a, b and c), based on literature values and computational results. Values limited by set range were not accepted. See table 1 for an exhaustive list of samples analyzed by FT-IR.

Table 1. Transmission-FT-IR analyzed sample systems in THF	
$Cr(CO)_3(\eta^6$-benzo-18-crown-6)	$Cr(CO)_3(\eta^6$-benzo-18-crown-6) + NaSCN
$Cr(CO)_3(\eta^6$-benzo-18-crown-6) + $NaB(ph)_4$	NaSCN
Benzene Chromium Tricarbonyl	Benzene Chromium Tricarbonyl + NaSCN

Chapter 3: Results and Discussion

Analysis of the computational data in conjunction with FT-IR spectra allows for a better understanding of the distribution of molecular species in solution as well as their vibrational modes and possible coupling among them. Ball and stick representations of the Gaussian 09

optimized molecules to be considered are included below in figure 12 for reference, as visualized by Molden software. Unless otherwise noted, all are shown in vacuum.

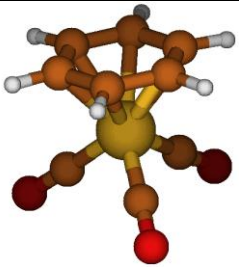

Benzene Chromium Tricarbonyl (BCT)

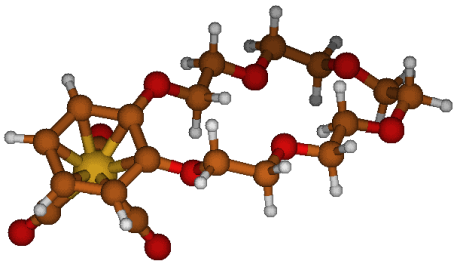

MB6-$Cr(CO)_3$

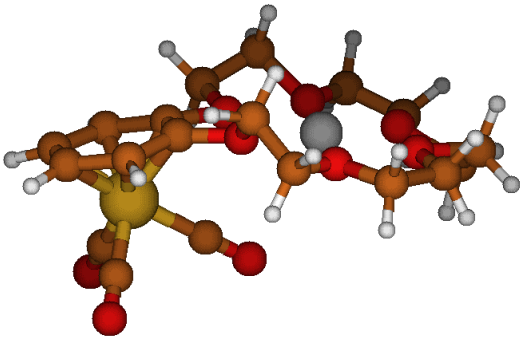

MB6-$Cr(CO)_3$-Na^+ (planer, unconverged)

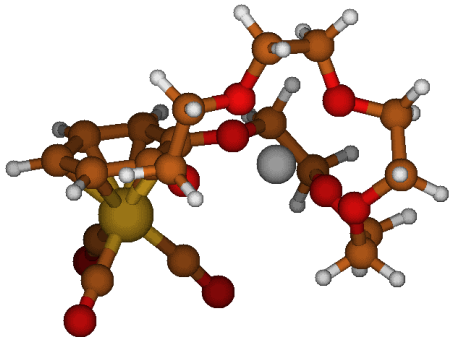

MB6-$Cr(CO)_3$-Na^+ (octahedral, converged)

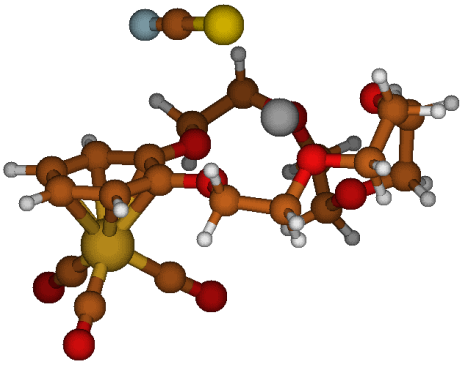

MB6-$Cr(CO)_3$-NaSCN (top)

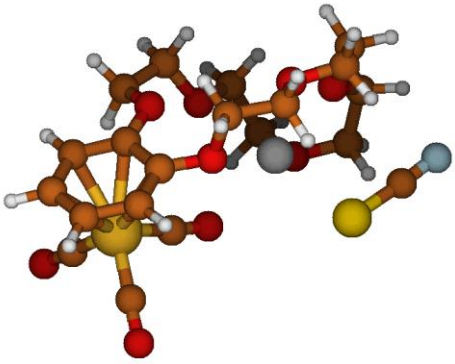

MB6-$Cr(CO)_3$-NaSCN (bottom)

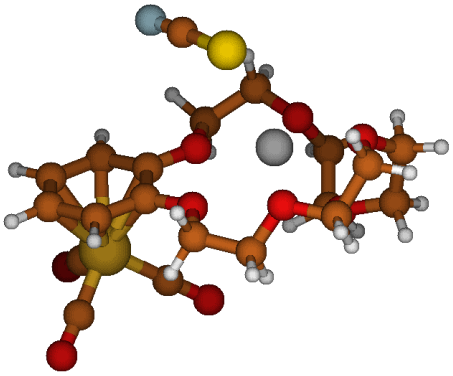

MB6-$Cr(CO)_3$-NaSCN in THF

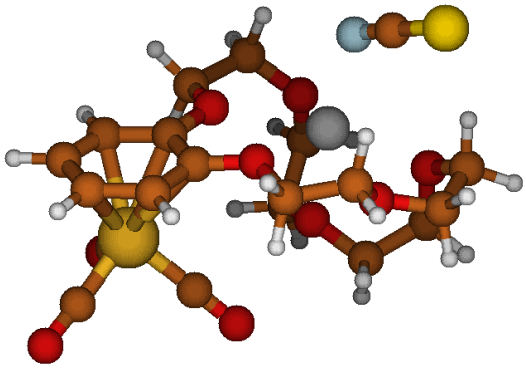

MB6-$Cr(CO)_3$-NaNCS

Figure 12. Minimized structures of considered molecules in vacuum unless noted.

Molecule	Min. Energy (hartree)	Calculated Vibrational Mode Frequencies (cm^{-1})					
		Asym. 1	Asym. 2	Asym Avg.	Δν	Symm.	SCN
MB6-$Cr(CO)_3$	-1075.43546	1904	1910	1907	6	1966	n/a
MB6-$Cr(CO)_3$-Na^+	-1663.94611	1923	1955	1939	33	1997	n/a
MB6-$Cr(CO)_3$-NaSCN (top)	-2155.22733	1876	1901	1889	25	1955	2073
MB6-$Cr(CO)_3$-NaSCN (bottom)	-2155.22537	1893	1922	1907	29	1971	2074
MB6-$Cr(CO)_3$-NaNCS	-2155.22781	1886	1903	1895	17	1959	2038
MB6-$Cr(CO)_3$-NaSCN in THF	-2155.26581	1831	1838	1834.5	7	1924	2058

Table 2. Minimized energy and calculated vibrational mode frequencies of considered molecules in vacuum unless otherwise noted. Frequencies have been scaled appropriately.

Molecule	Measured Vibrational Mode Frequencies (cm^{-1})							
	Asym. 1	Asym. 2	Asym Avg.	Δν	Symm.	SCN	SCN dimer	SCN triple
BCT	1891	1892	1891.5	1	1968	n/a	n/a	n/a
BCT with Na(SCN)	1891	1892	1891.5	1	1968	2056	2042	2072
MB6-$Cr(CO)_3$	1875	1881	1878	6	1959	n/a	n/a	n/a
MB6-$Cr(CO)_3$-$NaB(ph)_4$	1873	1886	1879.5	13	1962	n/a	n/a	n/a
MB6-$Cr(CO)_3$-NaSCN	1870	1883	1876.5	13	1958	2057	2043	2069
Na(SCN)	n/a	n/a	n/a	n/a	n/a	2056	2042	2076

Table 3. Measured FT-IR vibrational frequency data in THF, analyzed using Matlab R2009a.

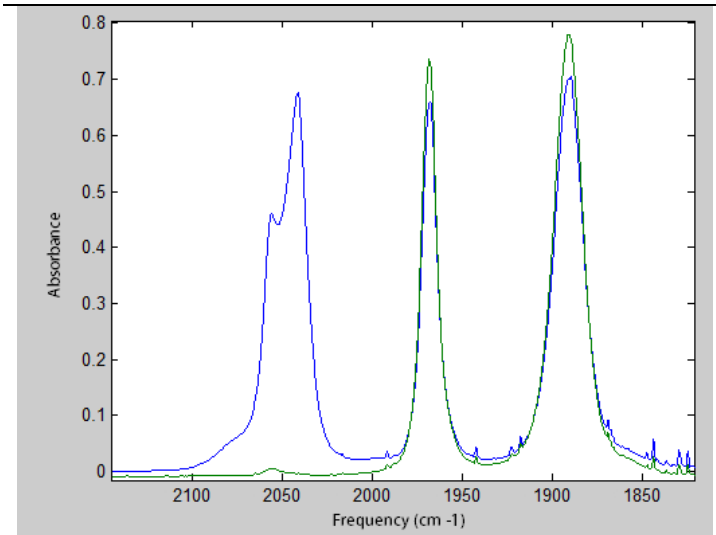

Figure 13. FT-IR spectra of BCT (green) and BCT with NaSCN (blue) in THF, overlain using Matlab.

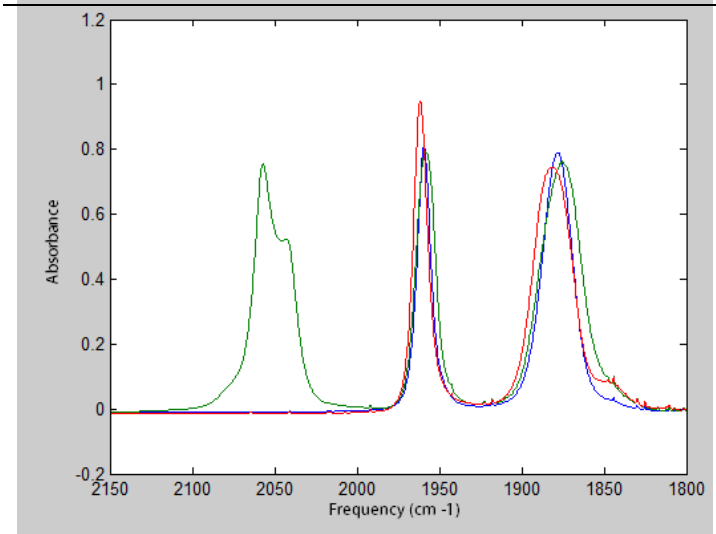

Figure 14. FT-IR spectra of MB6 (blue), MB6 with $NaB(ph)_4$ (red), and MB6 with NaSCN (green) in THF, overlain using Matlab.

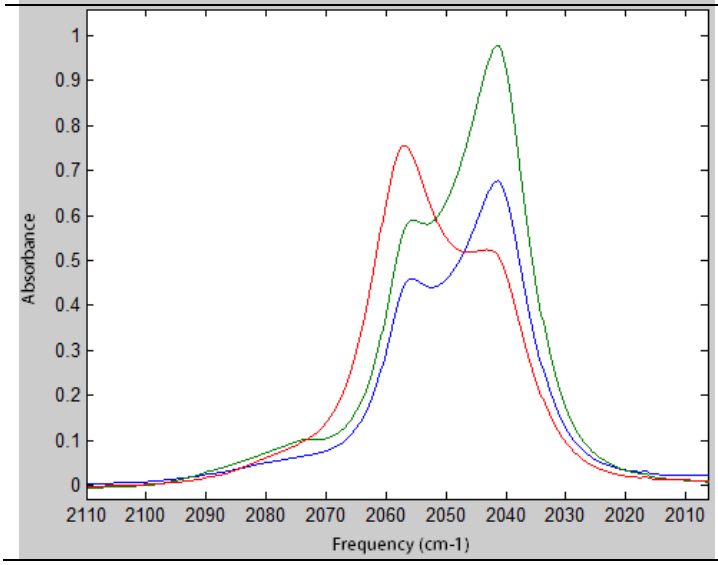

Figure 15. FT-IR spectra of NaSCN (green), BCT with NaSCN (blue), and MB6 with NaSCN (red) in THF, focusing on the thiocyanate absorptions. Spectra have been overlain using Matlab.

Generally speaking, there is be a total of four ways the crown can bind the Na(SCN) ion pair: either the opposite side or the same side as the chromium tricarbonyl (top or bottom, see figure 12), and as Na(SCN) or Na(NCS). Based on the calculated minimum molecular energies there is a preference for the SCN to exist on the top side of the complex (0.0020 Hartree or 5.3 kJ/mol) and to exist with a Na-N ionic linkage (0.0005 Hartree or 1.31 kJ/mol). These conclusions are also supported by crystallographic data and ion solvation studies.[1,17] Furthermore, the crown tends to bind the cation in an octahedral geometry rather than a more planar model which when tested failed to converge.

While this mode of complexation is likely representative of the vast majority of molecules in solution, the energetic difference between Na-thiocyanate configurations is quite small and it has been shown that Na(SCN) does in fact exist in solution in small concentrations.[17] This ion pair also created a larger splitting of the asymmetric carbonyl modes than Na(NCS) and absorbs at lower frequencies. Although minimal, these additional absorptions could interfere with data interpretation, and is likely evident in the tailing of the FT-IR spectrum of MB6-Na(SCN) in figure 14. This effect is not to be confused with the small peak in the same region which is evident in the MB6-NaB(ph)$_4$ spectrum since sodium tetraphenylborate has been documented to absorb at 1841 cm^{-1}.

The infrared absorbance spectrum of sodium thiocyanate itself is also rather complicated due to its tendency to form multi-ionic units in solution. In THF specifically, it has been reported that the most prevalent form is a dimer of two Na(NCS) contact pairs coordinating together, which absorbs at 2043 cm^{-1}, followed in concentration by the lone contact pair (2057 cm^{-1}), and finally a very small relative amount of triple ions (2074 cm^{-1}).[17] While the authors of this publication are quite sure of the first two assignments, they call into question the latter and leave

it ambiguous. Considering the data here, it is arguable that this small absorption is in actuality Na(SCN). Comparing the calculated vibrational frequencies of Na(SCN) and Na(NCS) in the context of the crown ether, their values of 2073 cm^{-1} and 2038 cm^{-1}, respectively, align quite well with experimental FT-IR data. Further support may be found in the tailing of the asymmetric carbonyl peak in complexed MB6, as previously discussed. Regardless of these points, however, detailed thiocyanate analysis allows for powerful assessment of the ionic environment of the moiety upon complexation in MB6-$Cr(CO)_3$. Absorbance at the frequency corresponding to the single contact pair is considerably stronger in the complex than with thiocyanate free in solution (see figure 15). Considering that the thiocyanate vibrational modes were not found to change frequency regardless of their complexation state, this assignment is quite probable. This is also good news since a multi-ion situation would complicate experiments on the complexed crown ether dramatically.

The carbonyl vibrational data also holds a great deal of information regarding the electronic structure and dynamics of the molecule. The symmetric mode frequency, when the molecule is complexed with $NaB(ph)_4$ increases by 3 cm^{-1} over the uncomplexed MB6. Since $[B(ph)_4]^-$ is such a sterically large counter-ion, the species forms a rather weak contact pair and $NaB(ph)_4$ may adequately model a free sodium cation when bound inside the crown. Therefore, the increase in carbonyl vibration frequency, which is also predicted by the DFT calculations, is directly correlated to electron withdraw by the cation ultimately from the carbonyl π^* orbitals. The catecholic oxygen atoms, however, which lie between the cation and the arene system, must be in the correct state in order to facilitate this coupling. Based on the trigonal planar geometry of these atoms, as seen in figure 12, they must express a significant amount of sp^2 hybridization character, which would allow the p-orbitals to interact openly with the π-system and create a

continuous path for electron withdrawal.[1] This effect may be visualized though molecular orbital representations, as seem in figure 17, created via Molden. After review of the entire calculated molecular orbital array, these specific examples were chosen to succinctly support their respective arguments while maintaining an accurate depiction of overall electron density.

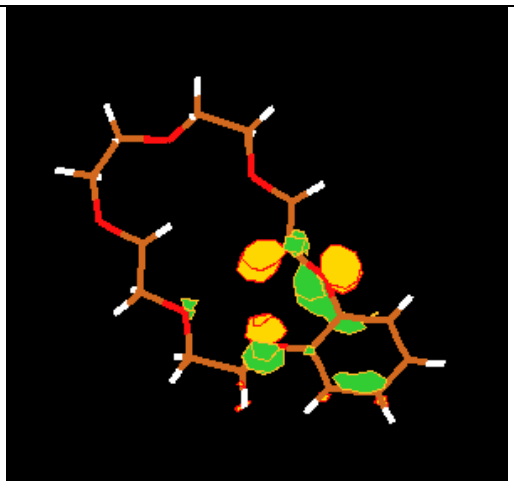

Figure 16. Indicative bonding orbital of MB6 representing minimal oxygen p-orbital interaction with the arene system

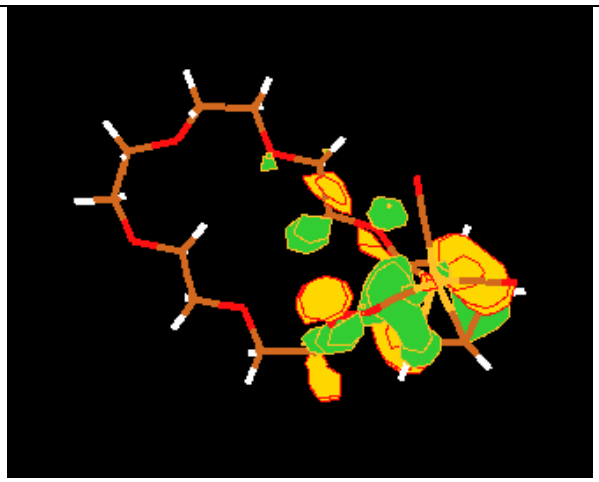

Figure 17. Indicative bonding orbital of MB6-$Cr(CO)_3Na^+$ representing direct and extensive oxygen p-orbital interaction with the arene system.

The frequency shift which follows the addition of Na(SCN) is a bit less intuitive. Even though the sp^2 hybridization still appears to contribute based on the geometry of the intermediate oxygen atoms, the symmetric and asymmetric carbonyl modes decrease in frequency experimentally and in theoretical models. The answer again lies in analysis of the molecular orbitals, as depicted in figure 18.

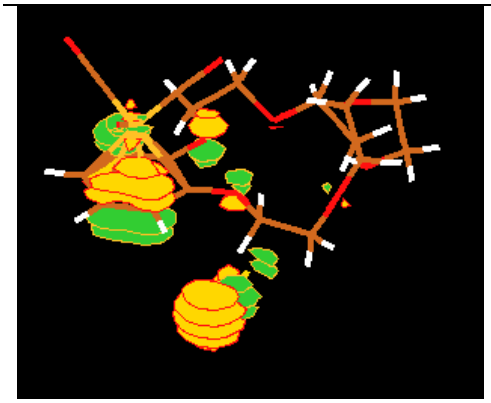

Figure 18. An occupied molecular orbital of MB6-$Cr(CO)_3$-NaSCN which shows electronic coupling between the thiocyanate moiety and the arene/ chromium system through an oxygen-arene π*orbital.

This occupied molecular orbital of MB6-$Cr(CO)_3$-NaSCN shows electronic coupling between the thiocyanate moiety and the arene/ chromium system through an oxygen-arene π*orbital. Since the oxygen-arene system exhibits added anti-bonding character, the electronic cross-talk between the crown and the chromium tricarbonyl system is reduced, thus hampering the ability of the sodium cation to withdraw electrons. In addition, the electron donation into the oxygen p-orbitals from the π-system is reduced, localizing electrons back into the metal system, and therefore the π* orbitals of the carbonyls overall reducing their frequency. This, however, is likely only one part of the overall interaction. One must also consider electrostatic effects and dielectric fields from solvent molecules, which were absent for this calculation. Even so, this example shows direct coupling between the thiocyanate and arene-chromium system.

In order to further prove the link between the carbonyl vibrational frequencies and the thiocyanate moiety, a set of ModRedundant scan calculations were carried out. The thiocyanate group was rotated about the central axis of the crown step-wise and the geometry was optimized at each point. The end goal was to monitor potential changes in electron density and vibrational modes through the scan, but due to time constraints, these final calculations were never carried out. However convergence was achieved after each of the 5 36° steps with minimal energy changes between them, showing that an analogue of this process is likely to occur in solution.

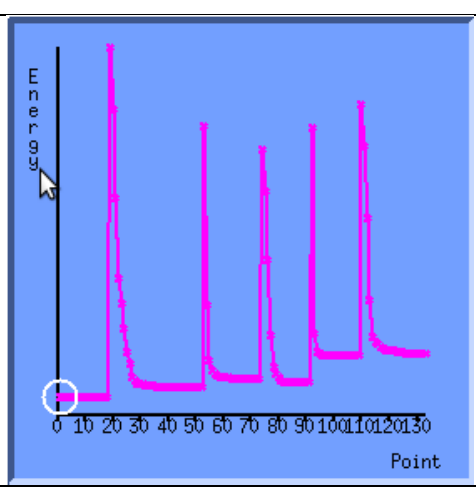

Step	Energy (Hartree)	ΔE (Hartree)	ΔE (kJ/mol)
t_0	-2155.227318	n/a	n/a
t_1	-2155.225852	+0.00147	+3.86
t_2	-2155.224704	+0.00115	+3.02
t_3	-2155.225277	-0.00057	-1.50
t_4	-2155.221352	+0.00393	+10.3
t_5	-2155.221122	+0.00023	+0.60

Figure 19. Energy profile of step-wise sweep of thiocyanate moiety around the crown. Minimized energy values and changes between each step are displayed above.

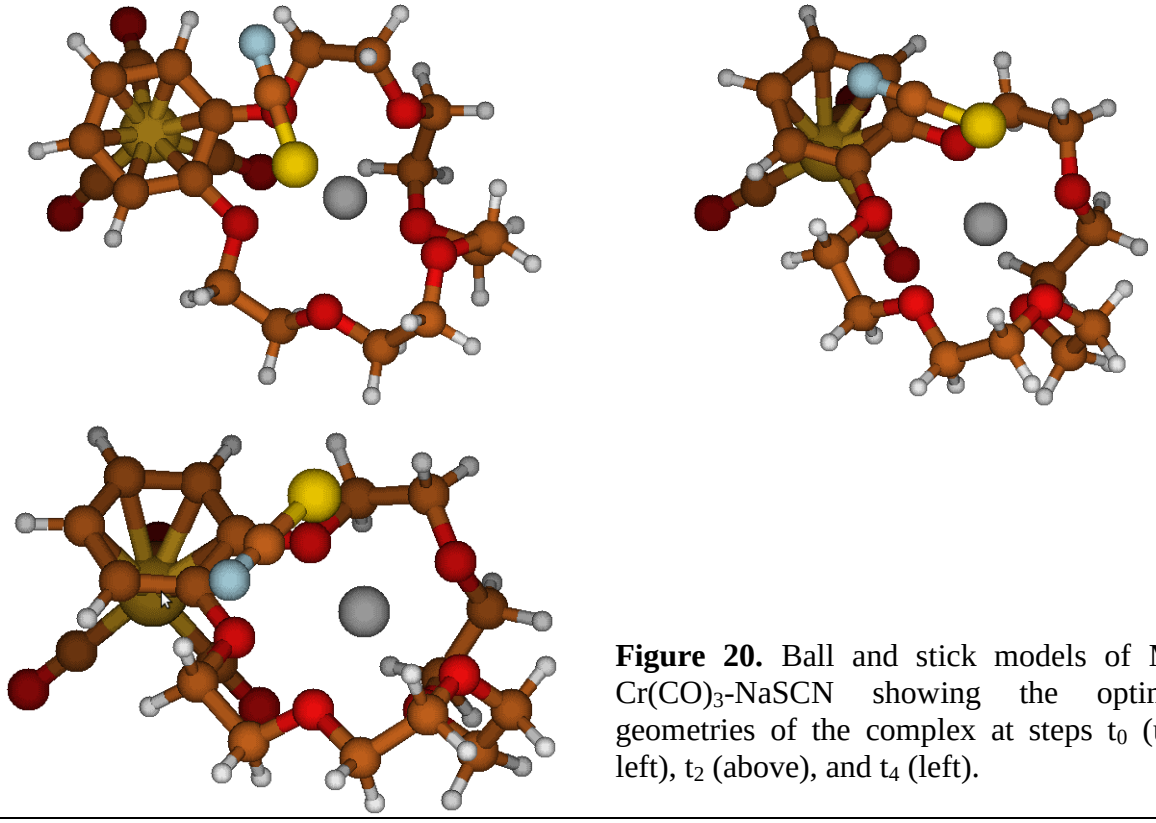

Figure 20. Ball and stick models of MB6-$Cr(CO)_3$-NaSCN showing the optimized geometries of the complex at steps t_0 (upper left), t_2 (above), and t_4 (left).

Chapter 4: Two-Dimensional Infrared Spectroscopy Experimentation

4.1 2DIR Background

Two-Dimensional Infrared spectroscopy (2DIR) is a non-linear technique which elicits a 3rd order response in sample media and is useful for correlating vibrational modes to study molecular dynamics and energy transfer.[18,19] The technique employs three non-collinear infrared pulses which first excite the sample then probe with the third. Figure 21visually represent this pulse sequence and label the key events.

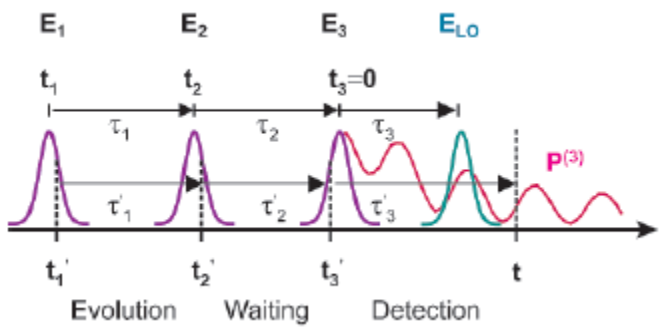

Figure 21. Pulse sequence and time variables for a 2DIR experiment.[18]

The first pulse, E_1, creates coherence among the molecule's vibrational modes between their respective ground and excited vibrational states during τ_1 or the Evolution of the system. The second pulse, E_2, brings the system into a population, which then decays according to a time constant over the waiting time. When the third pulse, E_3, interacts with the system, the states are again brought into coherence creating an oscillation and radiation of the third-order response ($P^{(3)}$).[18] The light emitted during coherence in the Evolution and Detection stages combined with a local oscillator pulse (E_{LO}) to be heterodyne detected. This process involves Fourier transformation of the time delay from the resulting transient interference pattern, resulting in the calculation of the correlated excitation and detection frequencies, ω_1 and ω_3, respectively. These frequencies are typically plotted as shown in figure 22.

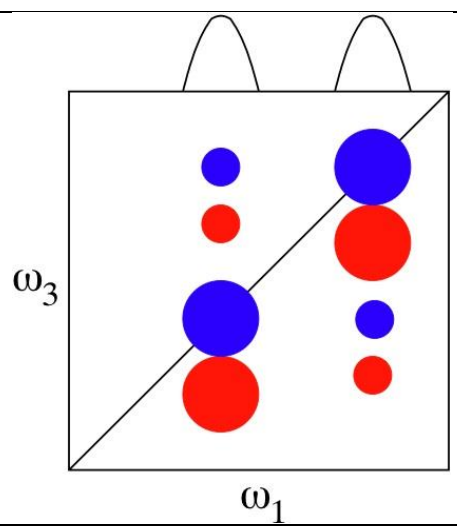

Figure 22. Idealized 2DIR spectrum involving two vibrational modes.

The peaks which appear along the diagonal, where ω_1 and ω_3 are equal, result when there is no chemical change in a molecule during the waiting time. These peaks would correspond to a 1D FT-IR spectrum if collapsed along the detection axis. However if there are chemical changes, including energy transfer between two coupled vibrational modes, off-diagonal "cross peaks" can appear. These detected frequencies may vary as a function of τ_2. Finally, the lower peaks (shown in red in figure 22) result from excitation to and emission from anharmonic higher energy levels.

4.2 Experimental Set-up

A Ti:sapphire laser, centered at 800 nm with a 1 kHz repetition rate generates horizontally polarized near IR pulses using β-barium borate (BBO) in a dual optical parametric amplifier (OPA) to combine a 0.8 mW seed pulse with a 25 W pump. This beam of 100 fs pulses is then used to generate two beams of mid-IR pulses via self-phase modulation and difference-frequency generation in separate GaSe crystals. One of these beams is split and carried through while the other is diverted off and not used in this experiment. The first beam is split in two and modulated in time via an interferometer-like set-up, becoming E_1 and E_2. The second is split three times, becoming E_3, a tracer, and the local oscillator (E_{LO}). The three input beams are arranged in "boxcar" geometry, as seen in figure 23, using the tracer beam as a stand-in for the signal output during alignment. The signal and E_{LO} are unconverted into the visible using $MgO:LiNbO_3$ in combination with an additional pump pulse via sum-frequency generation for detection by a 1340x100 pixel silicon CCD detector.[19]

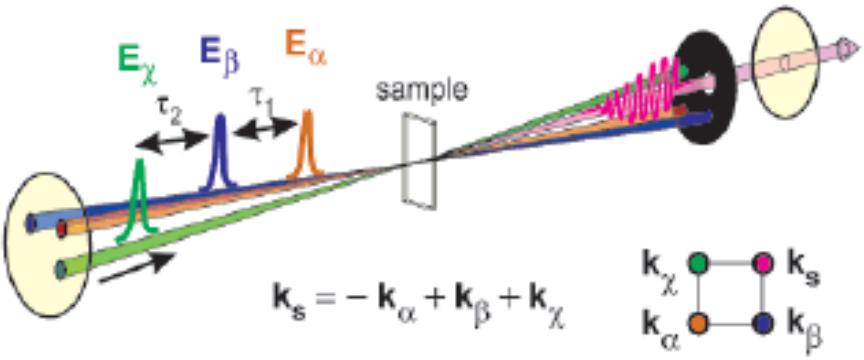

Figure 23. A schematic of boxcar geometry, also showing vector addition for detection of the rephrasing signal.[18]

4.3 Proposed Experiments

While the previous computational and FT-IR experiments provided a good foundation for the possibility of vibrational coupling and energy transfer, well-designed 2DIR experiments are necessary for detailed evaluation. The laser should be centered near 2000 cm^{-1} in order to simultaneously detect the absorptions of the carbonyl symmetric stretch and the thiocyanate anion. Some careful tuning may be necessary since these absorptions are separated by nearly 100 cm^{-1}, the bandwidth of the laser pulses. Sample mixtures including MB6-$Cr(CO)_3$ and $NaB(ph)_4$, MB6-$Cr(CO)_3$ and NaSCN, and BCT and NaSCN are of particular interest. Mixing with $NaB(ph)_4$ will provide a good "background" for removing sodium effects from the NaSCN trial and it will also be interesting to assess the possible coupling between the carbonyl absorption and that of $[B(ph)_4]^-$ to gauge the contact pair strength. Finally, a study of BCT with a high concentration of thiocyanate may illuminate any through-solvent coupling that could occur. The FT-IR spectra in figure 13appear to show a slight shift in absorbance frequency in this case, but could also be due to electrostatic interactions.

Chapter 5: Conclusion

Gaining a more thorough understanding of the dynamics of derivitized benzo-crown ethers will work to advance their application into meaningful areas, including biology and physiology. More generally, crown ethers are an excellent model system to study fundamental energy transfer and metal carbonyls themselves. Here, methods and results have been presented for the efficient synthesis, characterization and analysis of these important complexes. Several lines of evidence, including theoretical vibration and electron density calculations and FT-IR data, argue strongly for a dominant configuration in solution, as well as potential coupling between carbonyl and thiocyanate modes. It is unfortunate, however, that more powerful and conclusive 2DIR data could not be collected for this report. These experiments will provide crucial insight into the dynamics of the system and allow for continued application growth.

References

1. Anson, C.E., Creaser, C.S., and Stephenson, G.R., *J. Chem. Soc, Chem. Commun,* **1994,** *18,* 2175-76.
2. Budka, K., et. al., *J. Phys. Chem. A* **2008,** *112,* 10236-43.
3. Davidson, V.L., *Nature* **2011,** *3,* 662-63.
4. Stephenson, G.R., et. al., *Organometallics,* **1996,** *15,* 1451-56.
5. Gokel, G.W., Leevey, W.M, and Weber, M.E., *Chem Rev.* **2004,** *104,* 2723-50.
6. Shriver, D.F., *Inorganic Synthesis* **1979,** *XIX,* 154-58.
7. Hudecek, M., and Toma, S. *Journal of Organometallic Chemistry* **1990,** *393,* 115-8.
8. Hudecek, M., and Toma, S. *Journal of Organometallic Chemistry* **1991,** *406,* 147-51.
9. Hudecek, M., Gajda, V. and Toma, S. *Journal of Organometallic Chemistry* **1991,** *413,* 155-60.
10. Jaouen, G. et. al. *Journal of Organometallic Chemistry* **2005,** *690,* 847-56.
11. Skoog, D.A., Holler, F.J., and Crouch, S.R. *Principles of Instrumental Analysis 6th ed.* **2007,** Brooks/Cole Publishing, Belmost, Ca. pp. 498-518.
12. Franci, M.M., Pople, J.A., et. al. *J. Chem. Phys.* **1982,** *77,* 3654-65.
13. Frish, M.J., Pople, J.A., and Binkley, J.S. *J. Chem. Phys.* **1984,** *80,* 3265-69.
14. Spitznagel, G.W., et. al. *J. Comp. Chem,* **1987,** *8,* 1109-16.
15. Gaussian, Inc. Users' Reference. Available online at , <http://www.gaussian.com/g_tech/g_ur/g09help.htm>
16. Merrick, J.P., Moran, D., and Radom, L. *J. Phys. Chem. A* **2007,** *111,* 11683-700.
17. Saar, D., and Petrucci, S., *J. Phys. Chem.* **1986,** *90,* 3326-3330.
18. Khalil, M., Demirdoven, N., and Tokmakoff, A. *J. Phys. Chem. A* **2003,** *107,* 5258-79
19. Baiz, C. R, Nee, M. J., McCanne, R., Kubarych, K. J. *Opt. Lett.* **2008,** *33,* 2533-35.